Robustness of chiral surface current and subdominant *s*-wave Cooper pairs

Shu-Ichiro Suzuki◉ and Alexander A. Golubov

Faculty of Science and Technology and MESA+ Institute for Nanotechnology, University of Twente, 7500 AE Enschede, The Netherlands

The robustness of the chiral surface current of chiral superconductors against surface roughness is studied utilizing the quasiclassical Eilenberger theory. We consider the general chiral superconductors where the pair potential is given by the spherical harmonics Y_l^m such that the $(l, m) = (1, \pm 1)$ state corresponds to a $(p_x \pm ip_y)$-wave superconductor. The self-consistent calculations demonstrate that the robustness of the chiral current is determined by whether subdominant *s*-wave Cooper pairs are induced by disorder. The induced *s*-wave pairs act as an effective pair potential. As a result, the spontaneous chiral current of $(p_x + ip_y)$- and $(d_{x^2-y^2} + id_{xy})$-wave superconductors is robust against the roughness because the subdominant *s*-wave Cooper pairs are present.

I. INTRODUCTION

Chiral superconductivity is realized by Cooper pairs with finite orbital angular momenta. The nonzero angular momenta give rise to the so-called chiral current at a surface of a chiral superconductor (SC) spontaneously [1–18]. The direction of the chiral current is chosen by the Cooper-pair condensate with the spontaneous symmetry breaking. Observing the spontaneous surface current can be conclusive evidence to demonstrate the realization of chiral superconductivity. However, the spontaneous surface current has never been observed in any chiral SCs discovered so far [19,20].

The simplest chiral superconducting state is the $p_x + ip_y$-wave state (e.g., ^{3}He-A). The intrinsic total angular momentum in the $p_x + ip_y$-wave state has been a longstanding problem. In addition to the $p_x + ip_y$-wave state, other types of chiral SCs have been proposed as a pairing symmetry in several unconventional superconductors [11–18,21–23]. The possibility of the two-component *d*-wave superconductivity (e.g., $d_{x^2-y^2} + id_{xy}$-wave pairing) has been discussed in layered materials such as $Na_xCoO_2 \cdot yH_2O$ [24–28], doped graphene [29–32], and SrPtAs [33–37]. In addition, three-dimensional pairings for the two-component *d*-wave superconductivity are possible. The $d_{zx} + id_{yz}$-wave pairing has been discussed to reveal the superconductivity in a uranium compound URu_2Si_2 [38–40], and pnictide compound $LaPt_3P$ [41]. This pairing has recently been proposed as a new candidate for an unconventional SC Sr_2RuO_4 [18,42–49]. Furthermore, the possibility of the spin-triplet $f + if'$-wave superconductivity has been discussed to elucidate the superconductivity in UPt_3 [50–59].

To achieve the observation of the spontaneous chiral current, we cannot avoid the effects of surface roughness. In real-life experiments, the sample quality at a surface is not as specular as assumed in theoretical models. Although the total chiral current is estimated by assuming the secular surface [2,3], the surface roughness causes random reflections that are known to affect the surface Andreev bound states [5,7,14,18,60–63] in unconventional SCs such as high-T_c SCs. Indeed, it has been shown that the surface quality significantly

modifies the chiral current for higher-order chiral SCs [14]. Moreover, the suppression of the chiral current is deeply related to the pairing symmetry of the chiral SC. In the previous paper [18], the robustness of the chiral surface currents in the $p_x + ip_y$-wave and $d_{zx} + id_{yz}$-wave SCs has been compared. It has been demonstrated that the chiral current for a $p_x + ip_y$-wave SC can survive under the surface roughness, whereas that for the $d_{zx} + id_{yz}$-wave SC disappears even under weak roughness. The difference is well explained by the existence of the subdominant *s*-wave pairs at the surface. The *s*-wave pairs appear at a surface of the $p_x + ip_y$-wave SC and act as an effective pair potential, leading to the robust chiral surface current of the $p_x + ip_y$-wave SC. In the $d_{zx} + id_{yz}$-wave case, on the contrary, no *s*-wave pair is induced, resulting in the fragile surface chiral current.

In this paper, we examine the robustness of the spontaneous surface current in general chiral SCs, in particular, by focusing on the subdominant *s*-wave pairs at the surface. The
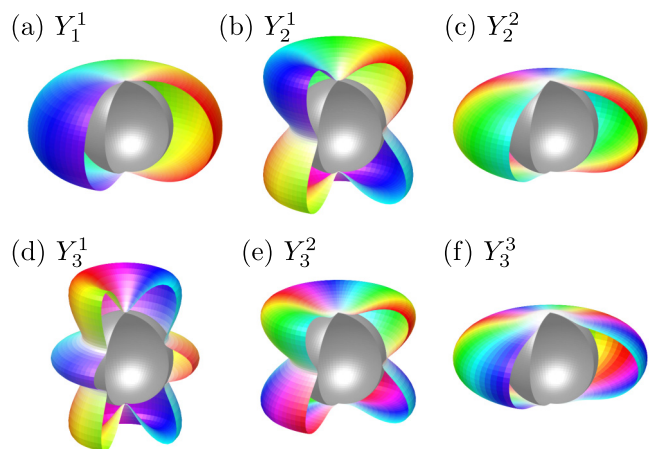
FIG. 1. Schematic superconducting gaps in the homogeneous limit. The superconducting gap of a general chiral superconductor is given by the spherical harmonics Y_l^m with $m > 0$. The color means the phase of the pair potential. The inner sphere indicates the Fermi sphere.
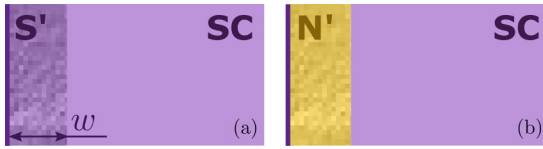
FIG. 2. Schematics of the systems. Superconductors with (a) rough surfaces and (b) dirty metallic surfaces. The disordered superconducting and normal-metal regions are indicated by S′ and N′. The surfaces are perpendicular to the x axis and located at $x = 0$ and L. The width of the disordered region is denoted by w.

pair potential is given in a general form using the spherical harmonics Y_l^m ($m \geqslant 1$), as shown in Fig. 1. Chiral SCs with rough surfaces and those covered with dirty normal metals are considered (Fig. 2). By solving the Eilenberger equation with the self-energy by random scatterings at the surface, the spatial profiles of the pair potentials, current density, and the s-wave pair amplitude are determined self-consistently.

We conclude that the chiral surface current in the Y_1^1, and Y_2^2, and Y_3^3 [i.e., $p_x + ip_y$-, $d_{x^2-y^2} + id_{xy}$-, and $f_{x(x^2-3y^2)} + if_{y(3x^2-y^2)}$-wave] SCs can survive under the strong-roughness limit. In particular, the chiral currents in Y_1^1 and Y_2^2 SCs are sufficiently large to be observed in experiments. The chiral current in the Y_3^3 SC remains finite, but may not be large enough to be detected. In the other chiral SCs, specular surfaces are required to observe the spontaneous current because the surface currents in these cases disappear even with a weak roughness. We also confirm that the subdominant s-wave Cooper pairs are essential for the observable spontaneous surface current by comparing the calculated current density with and without the subdominant s-wave Cooper pairs. We show that if there were no s-wave Cooper pairs, the spontaneous chiral currents for all chiral SCs could not survive, even under weak surface roughness. Namely, the robustness of the spontaneous current can be judged only by whether the subdominant s-wave Cooper pairs emerge.

II. QUASICLASSICAL EILENBERGER THEORY

We examine the effects of surface roughness utilizing the quasiclassical Eilenberger theory [64] in equilibrium [65]. The SC has a pair of parallel surfaces which are perpendicular to the x axis. The distance between two surfaces is denoted by L. The thin dirty regions and thin dirty normal metals with width w are introduced at the surfaces, as shown, respectively, in Figs. 2(a) and 2(b). The model in Fig. 2(b) is similar to the one that was first proposed by Ovchinnikov [66–68]. The Green's functions obey the Eilenberger equation, which is valid in the weak-coupling limit,

$$i\boldsymbol{v}_F \cdot \boldsymbol{\nabla} \check{g} + [i\omega_n \check{\tau}_3 + \check{H}, \check{g}]_- = 0, \quad (1)$$

$$\check{g} = \begin{pmatrix} \hat{g} & \hat{f} \\ -\hat{\underline{f}} & -\hat{\underline{g}} \end{pmatrix}, \quad \check{\Delta} = \begin{pmatrix} 0 & \hat{\Delta} \\ \hat{\underline{\Delta}} & 0 \end{pmatrix}, \quad (2)$$

$$\check{H} = \check{\Delta} + \check{\Sigma} = \begin{pmatrix} \hat{\xi} & \hat{\eta} \\ \hat{\underline{\eta}} & \hat{\underline{\xi}} \end{pmatrix}, \quad \check{\Sigma} = \frac{i}{2\tau_0} \langle \check{g} \rangle, \quad (3)$$

where $\langle \cdots \rangle = \int_0^\pi \int_{-\pi}^\pi \cdots \sin\theta \, d\varphi \, d\theta / 4\pi$ is the angle average on the Fermi sphere, the unit vector $\boldsymbol{k} =$

$(\sin\theta\cos\phi, \sin\theta\sin\phi, \cos\theta)$ represents the direction of the Fermi momentum, $\check{g} = \check{g}(\boldsymbol{r}, \boldsymbol{k}, i\omega_n)$ is the quasiclassical Green's function in the Matsubara representation, $\check{\Delta} = \check{\Delta}(\boldsymbol{r}, \boldsymbol{k})$ is the pair-potential matrix, and $\check{\Sigma} = \check{\Sigma}(\boldsymbol{r}, i\omega_n)$ is the self-energy with the mean free path $\ell = v_F \tau_0$. In this paper, the accents $\check{}$ and $\hat{}$ mean matrices in particle-hole and spin space. The identity matrices in particle-hole and spin space are, respectively, denoted by $\check{\tau}_0$ and $\hat{\sigma}_0$. The Pauli matrices are denoted by $\check{\tau}_\nu$ and $\hat{\sigma}_\nu$ with $\nu \in \{1, 2, 3\}$. All of the functions satisfy the symmetry relation $\hat{K}(\boldsymbol{r}, \boldsymbol{k}, i\omega_n) = [\hat{K}(\boldsymbol{r}, -\boldsymbol{k}, i\omega_n)]^*$. The effects of the vector potential are ignored because they only quantitatively affect the surface states. The quasiclassical Green's function is supplemented by the normalization condition

$$\check{g}\check{g} = \check{\tau}_0. \quad (4)$$

Throughout this paper, we use the units $k_B = \hbar = 1$.

The Eilenberger equation (1) can be simplified by the so-called Riccati parametrization [69–71]. The Green's function can be expressed in terms of the coherence function $\hat{\gamma} = \hat{\gamma}(\boldsymbol{r}, \boldsymbol{k}, i\omega_n)$,

$$\check{g} = 2 \begin{pmatrix} \hat{\mathcal{G}} & \hat{\mathcal{F}} \\ -\hat{\underline{\mathcal{F}}} & -\hat{\underline{\mathcal{G}}} \end{pmatrix} - \check{\tau}_3, \quad (5)$$

$$\hat{\mathcal{G}} = (1 - \hat{\gamma}\hat{\underline{\gamma}})^{-1}, \quad \hat{\mathcal{F}} = (1 - \hat{\gamma}\hat{\underline{\gamma}})^{-1}\hat{\gamma}. \quad (6)$$

The equation for $\hat{\gamma}$ is given by

$$(i\boldsymbol{v}_F \cdot \boldsymbol{\nabla} + 2i\omega_n)\hat{\gamma} + \hat{\underline{\xi}}\hat{\gamma} - \hat{\gamma}\hat{\underline{\xi}} - \hat{\eta} + \hat{\gamma}\hat{\underline{\eta}}\hat{\gamma} = 0. \quad (7)$$

Assuming no spin-dependent potential and single-spin $\hat{\Delta}$, we can parametrize the spin structure of the functions,

$$\hat{\Delta} = i\Delta_{\boldsymbol{k},\nu}(i\hat{\sigma}_\nu\hat{\sigma}_2), \quad (8)$$

$$\hat{\underline{\Delta}} = -i\Delta^*_{-\boldsymbol{k},\nu}(i\hat{\sigma}_\nu\hat{\sigma}_2)^* = i\Delta^*_{\boldsymbol{k},\nu}(i\hat{\sigma}_\nu\hat{\sigma}_2)^\dagger, \quad (9)$$

$$\hat{g} = g\hat{\sigma}_0, \quad \hat{f} = f_\nu(i\hat{\sigma}_\nu\hat{\sigma}_2), \quad \hat{\underline{f}} = f_\nu(i\hat{\sigma}_\nu\hat{\sigma}_2)^\dagger, \quad (10)$$

$$\hat{\eta} = i\eta_\nu(i\hat{\sigma}_\nu\hat{\sigma}_2), \quad \hat{\underline{\eta}} = i\eta_\nu(i\hat{\sigma}_\nu\hat{\sigma}_2)^\dagger, \quad (11)$$

where $\nu = 0$ ($\nu \in \{1, 2, 3\}$) is for the spin-singlet (spin-triplet) SC. In the following, we make ν explicit only when necessary. Equation (7) can be reduced to

$$\boldsymbol{v}_F \cdot \boldsymbol{\nabla}\gamma + 2\tilde{\omega}\gamma - \eta + \underline{\eta}\gamma^2 = 0, \quad (12)$$

$$\tilde{\omega} = \omega_n + \frac{\text{Re}\langle g \rangle}{2\tau_0}, \quad (13)$$

$$\eta_\nu = \Delta_{\boldsymbol{k}} + \frac{\langle f \rangle}{2\tau_0}, \quad \underline{\eta}_\nu = \Delta^*_{\boldsymbol{k}} - S_\nu \frac{\langle f \rangle^*}{2\tau_0}, \quad (14)$$

with $S_\nu = +1$ (-1) for the spin-triplet (spin-singlet) SC. In the homogeneous limit, γ is given by

$$\bar{\gamma}(\boldsymbol{k}, i\omega_n) = \frac{\Delta_{\boldsymbol{k}}}{\omega_n + \sqrt{\omega_n^2 + |\Delta_{\boldsymbol{k}}|^2}}, \quad (15)$$

where $\bar{}$ means the bulk value.

The pair potential of chiral superconductors is described by the two-component pair potential as summarized in Table I.

TABLE I. Momentum dependence of the pair potential and attractive potentials. We use the modified spherical harmonics so that $\max[Y_l^m(\boldsymbol{k})] = 1$. The amplitude of each component $\Delta_{1(2)}$ is determined by the self-consistent gap equation.

l	m	Δ	V_1	V_2
1	1	$\Delta_1 k_x + i\Delta_2 k_y$	$3k_x$	$3k_y$
2	1	$2(\Delta_1 k_x + i\Delta_2 k_y)k_z$	$(15/2)k_z k_x$	$(15/2)k_y k_z$
	2	$\Delta_1(k_x^2 - k_y^2) + 2i\Delta_2 k_x k_y$	$(15/4)(k_x^2 - k_y^2)$	$(15/2)k_x k_y$
3	1	$(\sqrt{135}/16)(\Delta_1 k_x + i\Delta_2 k_y)(5k_z^2 - 1)$	$(14/\sqrt{15})k_x(5k_z^2 - 1)$	$(14/\sqrt{15})k_y(5k_z^2 - 1)$
	2	$(\sqrt{27}/2)[\Delta_1(k_x^2 - k_y^2) + 2i\Delta_2 k_x k_y]k_z$	$(35/\sqrt{12})(k_x^2 - k_y^2)k_z$	$(70/\sqrt{12})k_x k_y k_z$
	3	$\Delta_1 k_x(k_x^2 - 3k_y^2) + i\Delta_2(3k_x^2 - k_y^2)k_y$	$(35/8)k_x(k_x^2 - 3k_y^2)$	$(35/8)(3k_x^2 - k_y^2)k_y$

Deep inside the superconductor, the momentum dependence of the pair potential is given by

$$\Delta_{\boldsymbol{k}} = \bar{\Delta}\tilde{Y}_l^m(\boldsymbol{k}), \qquad (16)$$

where we use the modified spherical harmonics $\tilde{Y}_l^m$ which satisfy $\max[\tilde{Y}_l^m(\boldsymbol{k})] = 1$. The chiral superconductivity is described by $m \geqslant 1$. The schematic gap amplitudes in the bulk are shown in Fig. 1, where the color means the phase of the pair potential $\arg[\Delta(\boldsymbol{k})]$ and the inner silver sphere means the Fermi sphere [72]. The spatial dependence of $\Delta_1(\boldsymbol{r})$ and $\Delta_2(\boldsymbol{r})$ is determined by the self-consistent gap equation which relates f and Δ,

$$\Delta_\mu(\boldsymbol{r}) = 2\lambda N_0 \frac{\pi}{i\beta} \sum_{\omega_n}^{\omega_c} \langle V_\mu(\boldsymbol{k}')f(\boldsymbol{r}, \boldsymbol{k}', i\omega_n)\rangle, \qquad (17)$$

where $\mu = 1$ or 2, $\beta = 1/T$, T_c is the critical temperature, N_0 is the density of the states (DOS) in the normal state at the Fermi energy, and n_c is the cutoff integer which satisfies $2n_c + 1 < \omega_c/\pi T < 2n_c + 3$. The attractive potentials V_1 and V_2 are also summarized in Table I. The coupling constant λ is finite in the superconducting region,

$$\lambda = \frac{1}{2N_0}\left[\ln\frac{T}{T_c} + \sum_{n=0}^{n_c}\frac{1}{n + 1/2}\right]^{-1}. \qquad (18)$$

In the normal metal, the coupling constant is set to $\lambda = 0$.

The spontaneous chiral current is calculated from the Green's function,

$$j_y(\boldsymbol{r}) = \sum_{\omega_n > 0}^{\omega_c} j_n, \qquad (19)$$

$$j_n = ev_F \frac{4\pi N_0}{\beta}\langle k_y \text{Im}[g(\boldsymbol{r}, \boldsymbol{k}, i\omega_n)]\rangle, \qquad (20)$$

with $e < 0$ is the charge of a quasiparticle.

In the numerical simulations, we fix the parameters as $L = 80\xi_0$, $w = 3\xi_0$, $\omega_c = 10\pi T_c$, and $T = 0.4T_c$, with $\xi_0 = v_F/2\pi T_c$ being the coherence length.

III. ROUGH SURFACE

We begin with the chiral surface current with rough surfaces as shown in Fig. 2(a). The partial chiral surface currents $j_{n=0}$ for each chiral SC are shown in Fig. 3. In the clean limit, the chiral surface currents for the $m = 1$ chiral SCs

(i.e., Y_1^1, Y_2^1, and Y_3^1) are sufficiently large to observe in experiments [2,19,20], as shown in Figs. 3(a), 3(b) and 3(d). On the other hand, the chiral surface currents for the $m > 1$ chiral SCs are smaller because the contributions from each chiral channel compensate each other [see Figs. 3(c), 3(e) and 3(f)] [12–17].

When the surface is rough, the chiral currents in the Y_2^1, Y_3^1, and Y_3^2 SCs disappear by the roughness shown in Figs. 3(b), 3(d) and 3(e), where the ratio of the coherence length and the mean free path is set to $\xi_0/\ell = 5$. On the other hand, the chiral currents in the Y_1^1, Y_2^2, and Y_3^3 SCs survive even under the rough surface [Figs. 3(a), 3(c) and 3(f)]. The chiral surface current in the Y_3^3 SC is, however, small in both the clean and rough-surface cases. Therefore, in a sample with nonspecular surfaces, we can observe the chiral surface current only when the sample is a Y_1^1 SC (i.e., $p_x + ip_y$-wave SC) or Y_2^2 SC (i.e., $d_{x^2-y^2} + id_{xy}$-wave SC).

In the previous paper [18], we pointed out that the subdominant s-wave Cooper pairs $\langle f\rangle$ play an important role under the disorder. The spatial dependences of the s-wave Cooper pairs $\langle f\rangle$ in each chiral SC are shown in Fig. 4, where $\omega_n = \omega_0$ and the strength of the disorder is set to $\xi_0/\ell = 0$, 1, or 5. In the Y_2^1 and Y_3^2 SCs (i.e., chiral SCs with fragile chiral currents), the amplitude of the s-wave Cooper pairs is exactly zero because of the k_z dependence of $\Delta_{\boldsymbol{k}} \sim k_z$ (therefore, the results are not shown). When the chiral current is robust, there are always s-wave Cooper pairs induced by the disorder. In the Y_1^1 and Y_2^2 cases, the large amplitude of the s-wave pairs $\langle f\rangle$ [Figs. 4(a) and 4(b)] results in the robust chiral surface current. The s-wave Cooper pairs act as an effective pair potential in the disordered region [see Eq. (14)] [73]. In this case, the internal interface between the clean and disordered region can be regarded as an interface between an effective s-wave SC and a chiral SC without a barrier potential. The quasiparticles feel this effective interface and give rise to the spontaneous current along it. In the chiral f-wave SCs (Y_3^1 and Y_3^3), the s-wave pairs in the disordered region are present, but the amplitude is much smaller than the Y_1^1 and Y_2^2 cases. The s-wave pairs have the largest amplitude inside the clean region ($x > w$). In this case, the s-wave pairs cannot affect the quasiparticle, as indicated by Eq. (14), because $\ell \to \infty$ in the clean region.

To examine the effect of the s-wave Cooper pairs $\langle f\rangle$, we calculate the chiral surface currents under the condition $\langle f\rangle = 0$ in Eq. (14). This condition is not realistic, but clarifies
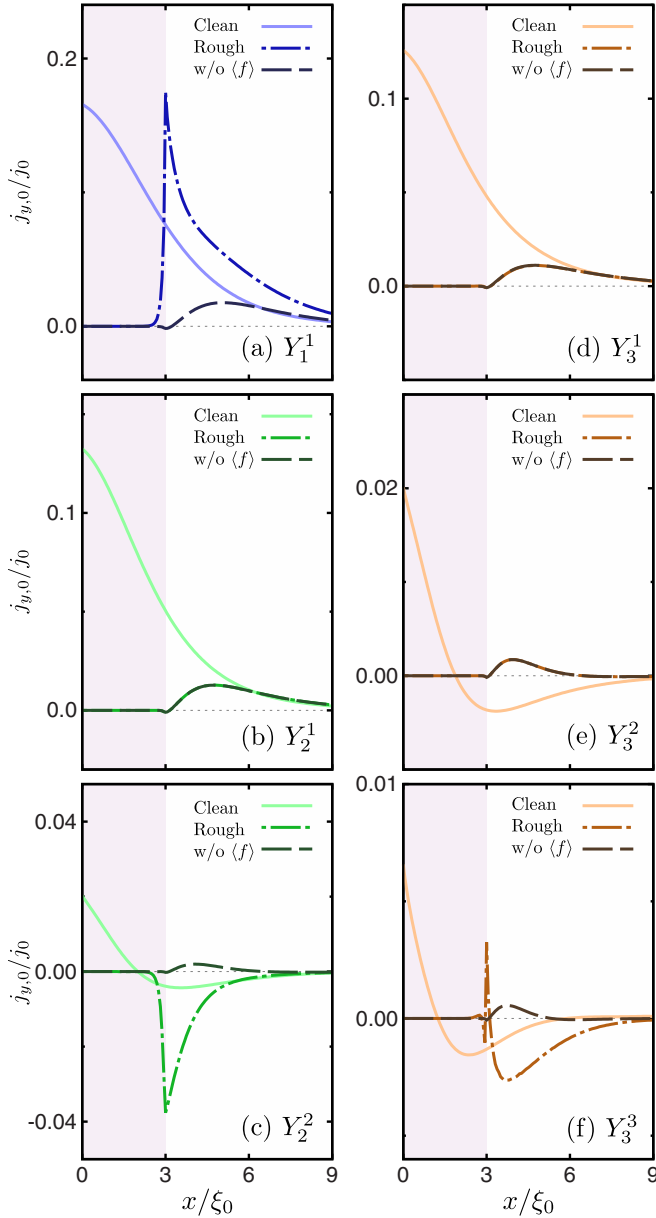
FIG. 3. Partial current densities at the lowest Matsubara frequency $j_{y,0}$ in each chiral SC. The results for the clean surface, rough surface, and rough surface without $\langle f \rangle$ are plotted with the solid (Clean), one-dot chain (Rough), and broken lines (w/o $\langle f \rangle$). The roughness parameters are set to $\xi_0/\ell = 5$ and $w = 3\xi_0$. The shaded regions indicate the surface disordered region. The pair potential is assumed to be (a) Y_1^1, (b) Y_2^1, (c) Y_2^2, (d) Y_3^1, (e) Y_3^2, and (f) Y_3^3. Note that the amplitude of the partial current density strongly depends on the pairing symmetry. When there are no s-wave Cooper pairs (i.e., $\langle f \rangle = 0$), the chiral current disappears in all chiral SCs. The current densities are normalized to $j_0 = |e| v_F \pi N_0 / \beta$. We fix the parameters as $L = 80\xi_0$, $w = 3\xi_0$, $\omega_c = 10\pi T_c$, and $T = 0.4T_c$.

the effect of the s-wave subdominant pairs $\langle f \rangle$. The results are shown in Fig. 3 with the broken lines. Even in the Y_1^1 SC, the chiral current is significantly suppressed if there are no s-wave Cooper pairs. The chiral currents in the Y_2^2 and Y_3^3 SCs are also significantly suppressed compared to the full calculation with $\langle f \rangle$. From these simulations, we conclude
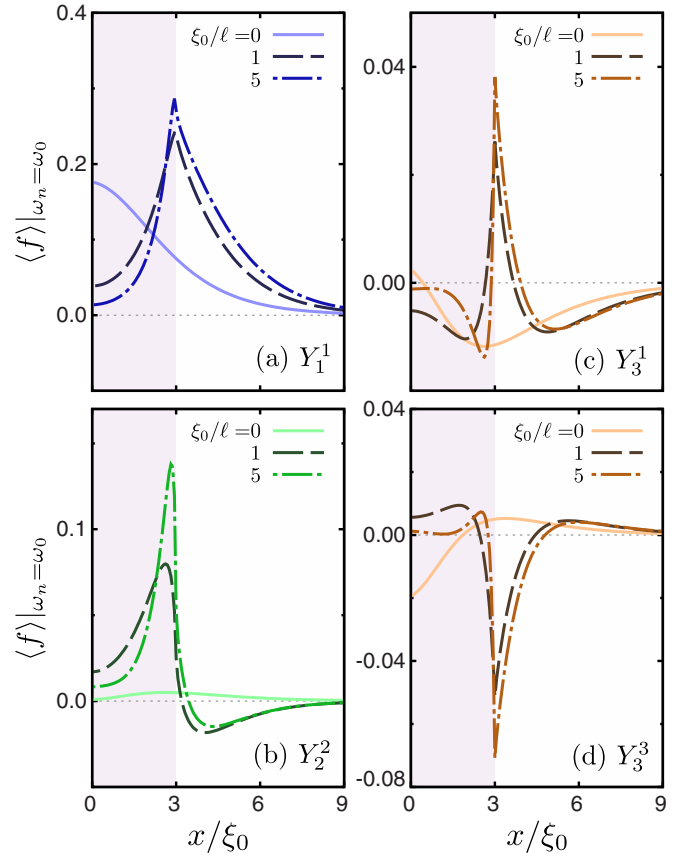
FIG. 4. Spatial profiles of the s-wave Cooper pairs $\langle f \rangle$ at ω_0. The strength of the roughness is set to $\xi_0/\ell = 0$, 1, and 5. The s-wave pairs have a large amplitude in the Y_1^1 SC. In (c),(d), the s-wave pairs have finite amplitudes in the disordered region, but smaller than those in (a),(b). We have confirmed that $\langle f \rangle = 0$ in the Y_2^1 and Y_3^2 SCs because $\Delta_{\boldsymbol{k}} \sim k_z$.

that the robust chiral current under surface roughness is supported by the s-wave subdominant Cooper pairs induced by the disorder.

The roughness dependences of the chiral surface current are shown in Fig. 5, where the parameters on the surface roughness are set to $w = 3\xi_0$ and $\xi_0/\ell = 0.0$, 0.2, 0.5, and 1.0. In the Y_1^1 and Y_2^2 case, the peak of the current density moves from the surface to the interface with increasing the roughness [Figs. 5(a) and 5(c)]. The chiral current in those SCs would be observed regardless of the surface quality of the sample. In the Y_3^3 case, the amplitude of the chiral current remains finite, even in the rough surface. However, the amplitude is small even in the clean limit. It is not clear if the chiral surface current in the Y_3^3 SC can be observed in experiments. When the s-wave pairs $\langle f \rangle$ are absent or sufficiently small, the chiral surface current is easily destroyed even by the weak roughness (e.g., $\ell > \xi_0$) [Figs. 5(b), 5(d) and 5(e)]. The observed chiral current would be much smaller than that estimated in the clean limit. Therefore, one needs to fabricated a sample with a sufficiently clean surface to observe the chiral current in these SCs.

The existence of the s-wave subdominant pairs also affects the pair potentials. The self-consistent pair potentials are shown in Fig. 6, where the strength of the disorder is set to $\xi_0/\ell = 5$. The results for the Y_1^1 and Y_2^2 are shown in
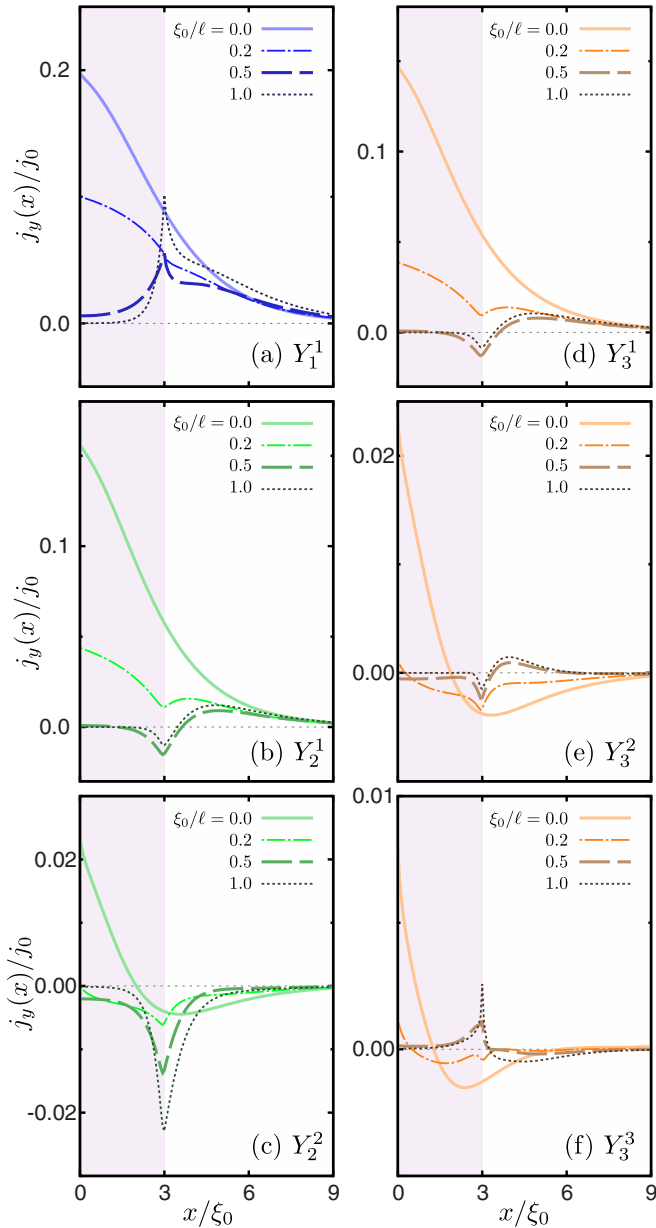
FIG. 5. Roughness dependence of the total current density in each chiral superconductor. The strength of the surface roughness is set to $\xi_0/\ell = 0$, 0.2, 0.5, and 1.0. The other parameters are set to the same values as used in Fig. 3. When the subdominant s-wave pairs are present, the chiral current flows along the internal interface as in (a), (c), and (f). On the other hand, the chiral current without the s-wave pairs is smeared out by the roughness as in (b), (d), and (e).

Figs. 6(a) and 6(b), and 6(c) and 6(d), respectively [74]. In the clean limit, the emergence of the Andreev bound states (ABSs) suppresses one of the pair potential, depending on the momentum dependence [see Figs. 6(a) and 6(c)] [2]. One of the pair potentials that changes its sign during the quasiparticle reflection at the surface (e.g., p_x-wave component of Y_1^1 SC) is responsible to form the ABSs [75]. Correspondingly, the other component of the pair potential is slightly enhanced at the surface [Figs. 6(b) and 6(c)]. When the surface is rough, both of the components are significantly suppressed. The chi-
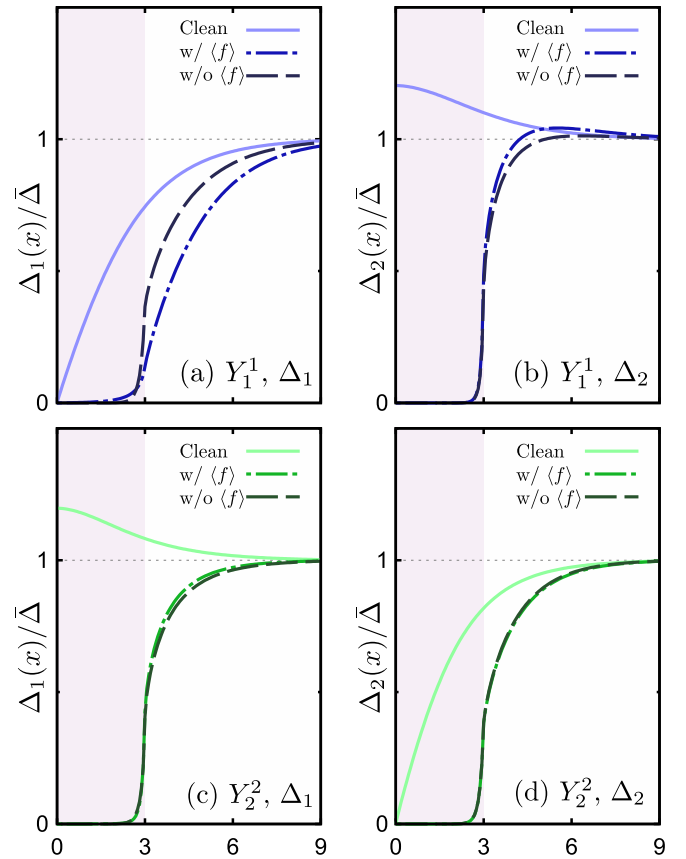
FIG. 6. Pair potentials for (a),(b) Y_1^1 and (e),(f) Y_2^2 superconductors. The first and second components are shown, respectively, in (a),(c) and (b),(d). The surface roughness significantly suppresses the pair potential near the surface. The amplitudes of the suppression depend on the presence of $\langle f \rangle$.

ral superconductivity is realized by anisotropic Cooper pairs, which are fragile against impurity scatterings (e.g., Anderson's theorem [76]). The roughness dependence of the pair potentials is discussed in the Appendix.

The calculated pair potentials without the s-wave pairs $\langle f \rangle$ are also shown in Fig. 6. In the Y_1^1 case, Δ_1 with $\langle f \rangle$ is smaller than that without $\langle f \rangle$. This behavior means the s-wave Cooper pairs induce the effective pair potential in the disordered region and make the internal interface an effective boundary. The other component of the pair potentials is also affected by the s-wave Cooper pairs. A similar behavior can be seen in the Y_2^2 case. Namely, Δ_2 with $\langle f \rangle$ is slightly more suppressed than the one without $\langle f \rangle$, whereas Δ_1 with $\langle f \rangle$ is slightly more enhanced than the one without $\langle f \rangle$. However, the effect is much smaller than the Y_1^1 case because the amplitude of the s-wave pairs is much smaller [see Fig. 4(b)]. We do not show the results for Y_2^1, Y_3^1, Y_3^2, and Y_3^3 because the s-wave subdominant pairs are absent or sufficiently small. The details of the spatial profiles of the pair potentials are discussed in the Appendix.

IV. NORMAL-METAL SURFACE

The surface roughness also affects the chiral surface current through modifying the pair potential near the surface.
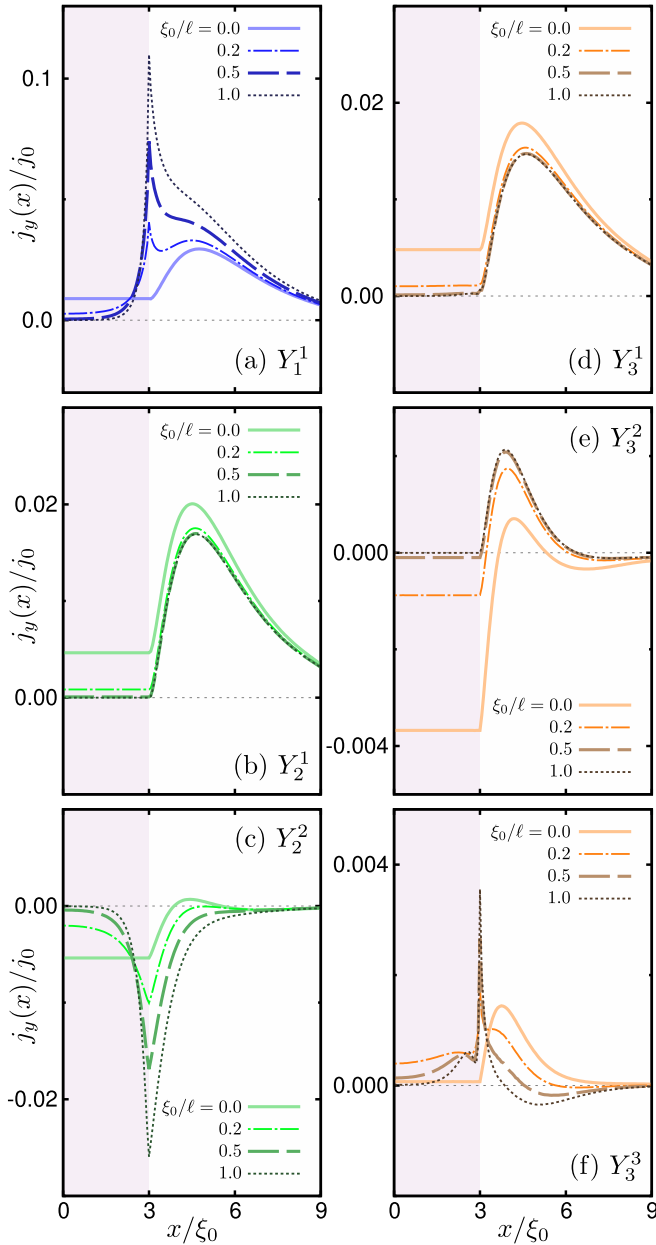
FIG. 7. Current density of each chiral SC with *normal* surfaces. The results are plotted in the same manner as in Fig. 3. When the *s*-wave pairs have a large amplitude, the chiral current can survive as in (a), (c), and (f).

To examine the effect through the pair potential, we have introduced the normal-metal surface [Fig. 2(b)], where the coupling constant is zero (i.e., $\Delta_{1(2)} = 0$). The chiral surface currents with a thin normal-metal surface are shown in Fig. 7, where the results are plotted in the same manner as in Fig. 5. We have confirmed that the pair potentials do not strongly depend on the roughness parameter ξ_0/ℓ (see the Appendix). The normal metal with $w = 3\xi_0$ is indicated by the shaded regions.

When the surface is in a clean-metallic state, the chiral surface current is small and would not be able to be measured in experiments regardless of the symmetry of the SC, as shown in Fig. 7 [9,10]. When the surface is a clean normal metal, j_y does not depend on x in the normal metal because of $\Delta = 0$.

Compared with that in a two-dimensional (2D) model [10], the surface effect in a 3D model is more prominent because there are more channels with the low injection angles. Those quasiparticles travel in the disordered region longer than those with high injection angles.

When the surface normal metal is disordered, the larger chiral current flows in the Y_1^1 SCs compared with the results with the clean-metal surface (i.e., $\xi_0/\ell = 0$). In the Y_2^2 and Y_3^3 SCs, the total current does not seem to change with increasing the roughness, even though the spatial dependence changes drastically. The current density in the Y_2^1, Y_3^1, and Y_3^2 SCs is simply suppressed with increasing the roughness. The difference comes from whether the *s*-wave pairs are present in the surface normal metal. As happened in the rough-surface SCs (Figs. 3–5), the *s*-wave subdominant pairs cause the effective superconductivity and the chiral current flows along the internal interface [Figs. 7(a), 7(c) and 7(f)]. When there is no (or significantly small) *s*-wave pairing in the normal metal, no effective superconductivity is expected; as a result, the chiral current does not arise along the internal interface [Figs. 7(b), 7(d) and 7(e)]. Note that a finite current flows inside the SC (e.g., Y_2^1 and Y_3^1) and similar profiles appear in the rough-surface model (Fig. 3). This current emerges because of the spatial gradient of the pair potential. This current density is, however, much smaller than those estimated in the clean limit.

Comparing the results with a rough surface and those with a normal-metal surface, we see that the existence of the *s*-wave subdominant pairs is essential for the observable chiral current. The suppression of the pair potential is less important than the presence of the *s*-wave pairs. Namely, we can judge the robustness of the chiral current by whether the *s*-wave pairs are induced as a subdominant Cooper pairs at a surface.

V. CONCLUSION

We have studied the effects of the surface roughness on the spontaneous chiral surface current of the general chiral SC utilizing the quasiclassical Eilenberger theory. We have considered a three-dimensional chiral SC with a rough or a dirty-normal-metallic surface, where the pair potential is generally described by the spherical harmonics Y_l^m with a finite magnetic quantum number ($m \neq 0$).

From the self-consistent solutions, the spontaneous current in Y_1^1 and Y_2^2 (i.e., $p_x + ip_y$- and $d_{x^2-y^2} + id_{xy}$-wave) SCs is sufficiently large to detect in experiments, even under the strong surface roughness. The spontaneous current in the Y_3^3 [i.e., $f_{x(x^2-3y^2)} + if_{y(3x^2-y^2)}$-wave] SC survives under the strong roughness, but might be too small to be observed. The surface chiral currents in Y_2^1, Y_3^1, and Y_3^2 SCs are easily destroyed even by weak surface roughness (i.e., $\ell > \xi_0$).

By comparing the calculated current densities with and without the subdominant *s*-wave Cooper pairs induced by the roughness, we have concluded that the robust chiral current is supported by the *s*-wave Cooper pairs. The *s*-wave Cooper pairs act as an effective pair potential in the disordered region. The current density in this case flows along the effective interface between the disordered and clean regions that can be regarded as an interface between an effective SC and the chiral SC.
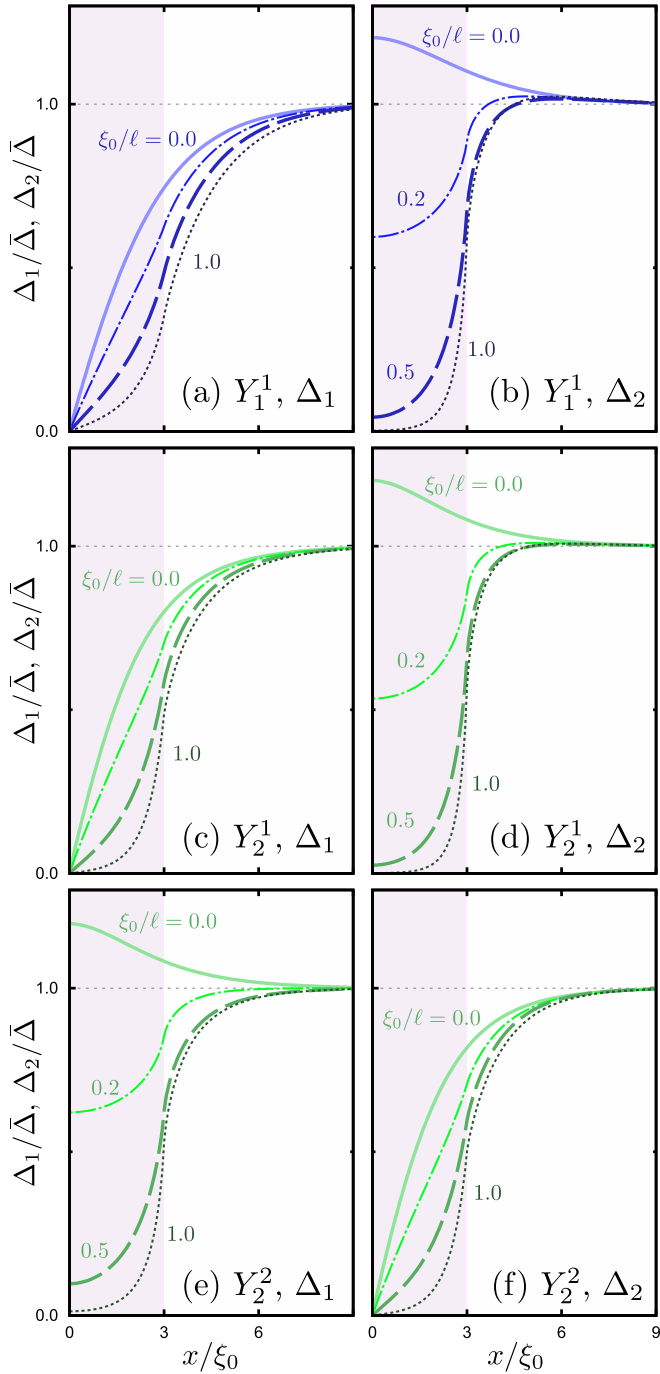
FIG. 8. Roughness dependence of the pair potentials for (a),(b) Y_1^1, (c),(d) Y_2^1, and (e),(f) Y_2^2. The first and second components are, respectively, shown in (a),(c),(e) and (b),(d),(f). The surface-roughness parameters are set to $w = 3\xi_0$, $\xi_0/\ell = 0.0$, 0.2, 0.5, and 1.0. The surface roughness significantly suppresses the pair potential.
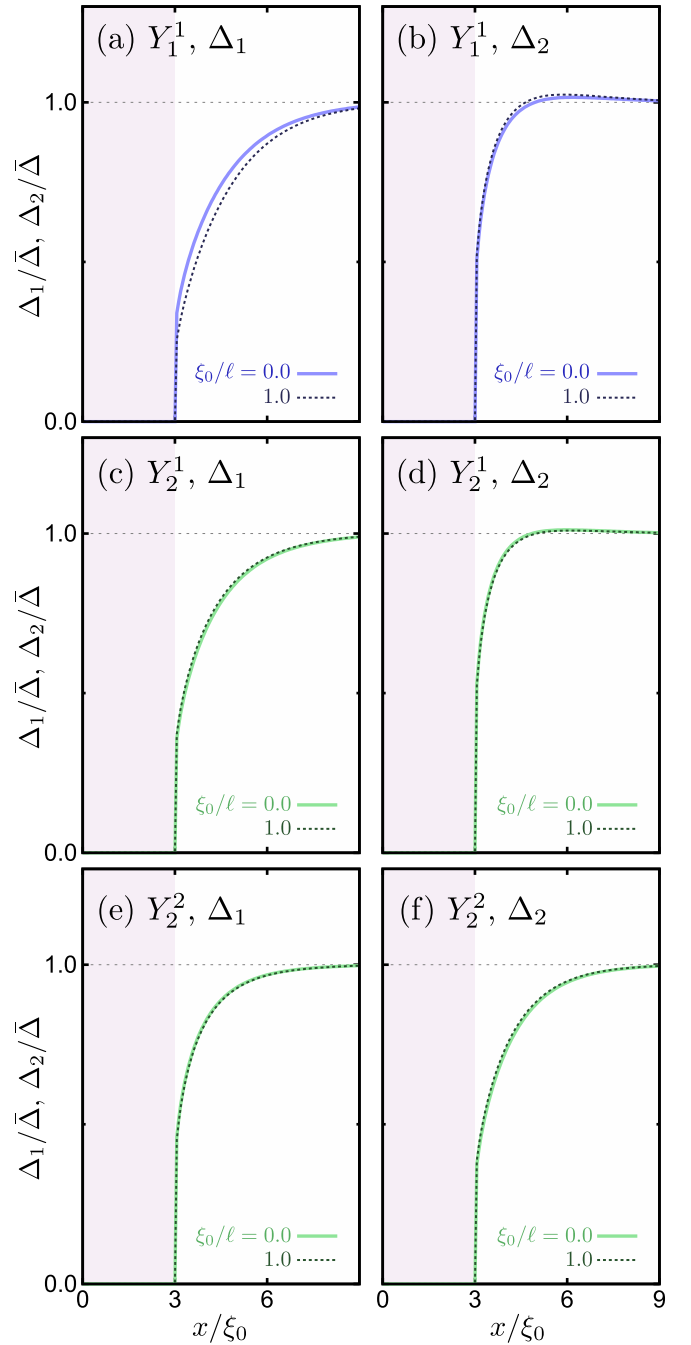
FIG. 9. Roughness dependence of the pair potentials with the thin dirty normal metal. The pair potentials are assumed to be (a),(b) Y_1^1, (c),(d) Y_2^1, and (e),(f) Y_2^2. The first and second components are, respectively, shown in (a),(c),(e) and (b),(d),(f). The surface-roughness parameters are set to $w = 3\xi_0$, $\xi_0/\ell = 0.0$, and 1.0. The results are plotted in the same manner as in Fig. 8.

APPENDIX: EFFECT OF THE SURFACE ROUGHNESS ON PAIR POTENTIALS

The spatial dependences of the pair potential in SCs with rough surfaces are shown in Fig. 8, where the strength of the roughness is set to $\xi_0/\ell = 0$, 0.2, 0.5, and 1.0. The pair potentials are suppressed by the surface roughness through the random scatterings. The suppression in the

pair potentials becomes more significant with increasing the roughness strength. The chiral superconductivity is realized with anisotropic Cooper pairing. The random quasiparticle scatterings kill such pairings with anisotropic momentum dependence. As a consequence, the pair potential decreases in the disordered region. The spatial dependences of the pair potentials of the Y_l^m SCs with $l = 3$ (not shown) are similar to those in the Y_2^1 SC because the amplitude of the s-wave pairs is zero or sufficiently small.

The spatial dependences of the pair potential in SCs with dirty-normal-metal surfaces are shown in Fig. 9, where the strength of the roughness is set to $\xi_0/\ell = 0$ or 1.0. Differing from the results with a rough surface, the pair potentials do not strongly depend on the strength of the roughness. The spatial dependences of the pair potentials of the Y_l^m SCs with $l = 3$ (not shown) are similar to those in the Y_2^1 SC because the amplitude of the s-wave pairs is zero or sufficiently small.

[1] T. Kita, Angular momentum of anisotropic superfluids at finite temperatures, J. Phys. Soc. Jpn. **67**, 216 (1998).

[2] M. Matsumoto and M. Sigrist, Quasiparticle states near the surface and the domain wall in a $p_x \pm ip_y$-wave superconductor, J. Phys. Soc. Jpn. **68**, 994 (1999).

[3] A. Furusaki, M. Matsumotoand, and M. Sigrist, Spontaneous Hall effect in a chiral p-wave superconductor, Phys. Rev. B **64**, 054514 (2001).

[4] M. Stone and R. Roy, Edge modes, edge currents, and gauge invariance in $p_x + ip_y$ superfluids and superconductors, Phys. Rev. B **69**, 184511 (2004).

[5] Y. Nagato, S. Higashitani, and K. Nagai, Subgap in the edge states of two-dimensional chiral superconductor with rough surface, J. Phys. Soc. Jpn. **80**, 113706 (2011).

[6] J. A. Sauls, Surface states, edge currents, and the angular momentum of chiral p-wave superfluids, Phys. Rev. B **84**, 214509 (2011).

[7] S. V. Bakurskiy, A. A. Golubov, M. Yu. Kupriyanov, K. Yada, and Y. Tanaka, Anomalous surface states at interfaces in p-wave superconductors, Phys. Rev. B **90**, 064513 (2014).

[8] A. Bouhon and M. Sigrist, Current inversion at the edges of a chiral p-wave superconductor, Phys. Rev. B **90**, 220511(R) (2014).

[9] S. Lederer, W. Huang, E. Taylor, S. Raghu, and C. Kallin, Suppression of spontaneous currents in Sr_2RuO_4 by surface disorder, Phys. Rev. B **90**, 134521 (2014).

[10] S. V. Bakurskiy, N. V. Klenov, I. I. Soloviev, M. Yu. Kupriyanov, and A. A. Golubov, Observability of surface currents in p-wave superconductors, Supercond. Sci. Technol. **30**, 044005 (2017).

[11] B. Braunecker, P. A. Lee, and Z. Wang, Edge currents in superconductors with a broken time-reversal symmetry, Phys. Rev. Lett. **95**, 017004 (2005).

[12] W. Huang, E. Taylor, and C. Kallin, Vanishing edge currents in non-p-wave topological chiral superconductors, Phys. Rev. B **90**, 224519 (2014).

[13] Y. Tada, W. Nie, and M. Oshikawa, Orbital angular momentum and spectral flow in two-dimensional chiral superfluids, Phys. Rev. Lett. **114**, 195301 (2015).

[14] S.-I. Suzuki and Y. Asano, Spontaneous edge current in a small chiral superconductor with a rough surface, Phys. Rev. B **94**, 155302 (2016).

[15] X. Wang, Z. Wang, and C. Kallin, Spontaneous edge current in higher chirality superconductors, Phys. Rev. B **98**, 094501 (2018).

[16] E. Sugiyama and S. Higashitani, Surface bound states and spontaneous edge currents in chiral superconductors: Effect of spatially varying order parameter, J. Phys. Soc. Jpn. **89**, 034706 (2020).

[17] W. Nie, W. Huang, and H. Yao, Edge current and orbital angular momentum of chiral superfluids revisited, Phys. Rev. B **102**, 054502 (2020).

[18] S.-I. Suzuki, S. Ikegaya, and A. A. Golubov, Destruction of surface states of $(d_{zx} + id_{yz})$-wave superconductor by surface roughness: Application to Sr_2RuO_4, Phys. Rev. Res. **4**, L042020 (2022).

[19] P. G. Björnsson, Y. Maeno, M. E. Huber, and K. A. Moler, Scanning magnetic imaging of Sr_2RuO_4, Phys. Rev. B **72**, 012504 (2005).

[20] J. R. Kirtley, C. Kallin, C. W. Hicks, E.-A. Kim, Y. Liu, K. A. Moler, Y. Maeno, and K. D. Nelson, Upper limit on spontaneous supercurrents in Sr_2RuO_4, Phys. Rev. B **76**, 014526 (2007).

[21] S. Kobayashi, Y. Tanaka, and M. Sato, Fragile surface zero-energy flat bands in three-dimensional chiral superconductors, Phys. Rev. B **92**, 214514 (2015).

[22] S. Tamura, S. Kobayashi, L. Bo, and Y. Tanaka, Theory of surface Andreev bound states and tunneling spectroscopy in three-dimensional chiral superconductors, Phys. Rev. B **95**, 104511 (2017).

[23] S.-I. Suzuki, M. Sato, and Y. Tanaka, Identifying possible pairing states in Sr_2RuO_4 by tunneling spectroscopy, Phys. Rev. B **101**, 054505 (2020).

[24] A. Tanaka and X. Hu, Possible spin triplet superconductivity in $Na_xCoO_2 \cdot yH_2O$, Phys. Rev. Lett. **91**, 257006 (2003).

[25] G. Baskaran, Electronic model for CoO_2 layer based systems: Chiral resonating valence bond metal and superconductivity, Phys. Rev. Lett. **91**, 097003 (2003).

[26] K. Takada, H. Sakurai, E. Takayama-Muromachi, F. Izumi, R. A. Dilanian, and T. Sasaki, Superconductivity in two-dimensional CoO_2 layers, Nature (London) **422**, 53 (2003).

[27] M. Ogata, Superconducting states in frustrating $t - J$ model: A model connecting high-T_c cuprates, organic conductors and Na_xCoO_2, J. Phys. Soc. Jpn. **72**, 1839 (2003).

[28] M. L. Kiesel, C. Platt, W. Hanke, and R. Thomale, Model evidence of an anisotropic chiral d+id-wave pairing state for the water-intercalated $Na_xCoO_2 \cdot yH_2O$ superconductor, Phys. Rev. Lett. **111**, 097001 (2013).

[29] M. L. Kiesel, C. Platt, W. Hanke, D. A. Abanin, and R. Thomale, Competing many-body instabilities and unconventional superconductivity in graphene, Phys. Rev. B **86**, 020507(R) (2012).

[30] A. M. Black-Schaffer, Edge properties and Majorana fermions in the proposed chiral d-wave superconducting state of doped graphene, Phys. Rev. Lett. **109**, 197001 (2012).

[31] R. Nandkishore, L. S. Levitov, and A. V. Chubukov, Chiral superconductivity from repulsive interactions in doped graphene, Nat. Phys. **8**, 158 (2012).

[32] A. M. Black-Schaffer and C. Honerkamp, Chiral *d*-wave superconductivity in doped graphene, J. Phys.: Condens. Matter **26**, 423201 (2014).

[33] P. K. Biswas, H. Luetkens, T. Neupert, T. Stürzer, C. Baines, G. Pascua, A. P. Schnyder, M. H. Fischer, J. Goryo, M. R. Lees, H. Maeter, F. Brückner, H.-H. Klauss, M. Nicklas, P. J. Baker, A. D. Hillier, M. Sigrist, A. Amato, and D. Johrendt, Evidence for superconductivity with broken time-reversal symmetry in locally noncentrosymmetric SrPtAs, Phys. Rev. B **87**, 180503(R) (2013).

[34] M. H. Fischer, T. Neupert, C. Platt, A. P. Schnyder, W. Hanke, J. Goryo, R. Thomale, and M. Sigrist, Chiral *d*-wave superconductivity in SrPtAs, Phys. Rev. B **89**, 020509(R) (2014).

[35] J. F. Landaeta, S. V. Taylor, I. Bonalde, C. Rojas, Y. Nishikubo, K. Kudo, and M. Nohara, High-resolution magnetic penetration depth and inhomogeneities in locally noncentrosymmetric SrPtAs, Phys. Rev. B **93**, 064504 (2016).

[36] J. Goryo, Y. Imai, W. B. Rui, M. Sigrist, and A. P. Schnyder, Surface magnetism in a chiral *d*-wave superconductor with hexagonal symmetry, Phys. Rev. B **96**, 140502(R) (2017).

[37] H. Ueki, R. Tamura, and J. Goryo Possibility of chiral *d*-wave state in the hexagonal pnictide superconductor SrPtAs, Phys. Rev. B **99**, 144510 (2019).

[38] Y. Kasahara, T. Iwasawa, H. Shishido, T. Shibauchi, K. Behnia, Y. Haga, T. D. Matsuda, Y. Onuki, M. Sigrist, and Y. Matsuda, Exotic superconducting properties in the electron-hole-compensated heavy-fermion semimetal URu_2Si_2, Phys. Rev. Lett. **99**, 116402 (2007).

[39] Y. Kasahara, H. Shishido, T. Shibauchi, Y. Haga, T. D. Matsuda, Y. Onuki, and Y. Matsuda, Superconducting gap structure of heavy-Fermion compound URu_2Si_2 determined by angle-resolved thermal conductivity, New J. Phys. **11**, 055061 (2009).

[40] S. Kittaka, Y. Shimizu, T. Sakakibara, Y. Haga, E. Yamamoto, Y. Ōnuki, Y. Tsutsumi, T. Nomoto, H. Ikeda, and K. Machida, Evidence for chiral d-wave superconductivity in URu_2Si_2 from the field-angle variation of its specific heat, J. Phys. Soc. Jpn. **85**, 033704 (2016).

[41] P. K. Biswas, S. K. Ghosh, J. Z. Zhao, D. A. Mayoh, N. D. Zhigadlo, X. Xu, C. Baines, A. D. Hillier, G. Balakrishnan, and M. R. Lees, Chiral singlet superconductivity in the weakly correlated metal $LaPt_3P$, Nat. Commun. **12**, 2504 (2021).

[42] Y. Maeno, H. Hashimoto, K. Yoshida, S. Nishizaki, T. Fujita, J. G. Bednorz, and F. Lichtenberg, Superconductivity in a layered perovskite without copper, Nature (London) **372**, 532 (1994).

[43] A. P. Mackenzie and Y. Maeno, The superconductivity of Sr_2RuO_4 and the physics of spin-triplet pairing, Rev. Mod. Phys. **75**, 657 (2003).

[44] A. Pustogow, Y. Luo, A. Chronister, Y.-S. Su, D. A. Sokolov, F. Jerzembeck, A. P. Mackenzie, C. W. Hicks, N. Kikugawa, S. Raghu, E. D. Bauer, and S. E. Brown, Constraints on the superconducting order parameter in Sr_2RuO_4 from oxygen-17 nuclear magnetic resonance, Nature (London) **574**, 72 (2019).

[45] H. G. Suh, H. Menke, P. M. R. Brydon, C. Timm, A. Ramires, and D. F. Agterberg, Stabilizing even-parity chiral superconductivity in Sr_2RuO_4, Phys. Rev. Res. **2**, 032023(R) (2020).

[46] Y. Fukaya, T. Hashimoto, M. Sato, Y. Tanaka, and K. Yada, Spin susceptibility for orbital-singlet Cooper pair in the three-dimensional Sr2RuO4 superconductor, Phys. Rev. Res. **4**, 013135 (2022).

[47] V. Grinenko, S. Ghosh, R. Sarkar, J.-C. Orain, A. Nikitin, M. Elender, D. Das, Z. Guguchia, F. Brückner, M. E. Barber, J. Park, N. Kikugawa, D. A. Sokolov, J. S. Bobowski, T. Miyoshi, Y. Maeno, A. P. Mackenzie, H. Luetkens, C. W. Hicks, and H.-H. Klauss, Split superconducting and time-reversal symmetry-breaking transitions in Sr_2RuO_4 under stress, Nat. Phys. **17**, 748 (2021).

[48] V. Grinenko, D. Das, R. Gupta, B. Zinkl, N. Kikugawa, Y. Maeno, C. W. Hicks, H.-H. Klauss, M. Sigrist, and R. Khasanov, Unsplit superconducting and time reversal symmetry breaking transitions in Sr_2RuO_4 under hydrostatic pressure and disorder, Nat. Commun. **12**, 3920 (2021).

[49] S. Ikegaya, S.-I. Suzuki, Y. Tanaka, and D. Manske, Proposal for identifying possible even-parity superconducting states in Sr_2RuO_4 using planar tunneling spectroscopy, Phys. Rev. Res. **3**, L032062 (2021).

[50] R. A. Fisher, S. Kim, B. F. Woodfield, N. E. Phillips, L. Taillefer, K. Hasselbach, J. Flouquet, A. L. Giorgi, and J. L. Smith, Specific heat of UPt_3: Evidence for unconventional superconductivity, Phys. Rev. Lett. **62**, 1411 (1989).

[51] C. H. Choi and J. A. Sauls, Identification of odd-parity superconductivity in UPt_3 from paramagnetic effects on the upper critical field, Phys. Rev. Lett. **66**, 484 (1991).

[52] J. A. SaulsA theory for the superconducting phases of UPt_3, J. Low Temp. Phys. **95**, 153 (1994).

[53] K. Machida, T. Nishira, and T. Ohmi, Orbital symmetry of a triplet pairing in a heavy fermion superconductor UPt_3, J. Phys. Soc. Jpn. **68**, 3364 (1999).

[54] Matthias J. Graf, S.-K. Yip, and J. A. Sauls, Identification of the orbital pairing symmetry in UPt_3, Phys. Rev. B **62**, 14393 (2000).

[55] R. Joynt and L. Taillefer, The superconducting phases of UPt3, Rev. Mod. Phys. **74**, 235 (2002).

[56] Y. Machida, A. Itoh, Y. So, K. Izawa, Y. Haga, E. Yamamoto, N. Kimura, Y. Onuki, Y. Tsutsumi, and K. Machida, Twofold spontaneous symmetry breaking in the heavy-fermion superconductor UPt_3, Phys. Rev. Lett. **108**, 157002 (2012).

[57] Y. Tsutsumi, K. Machida, T. Ohmi, and M. Ozaki, A spin triplet superconductor UPt_3, J. Phys. Soc. Jpn. **81**, 074717 (2012).

[58] K. Izawa, Y. Machida, A. Itoh, Y. So, K. Ota, Y. Haga, E. Yamamoto, N. Kimura, Y. Onuki, Y. Tsutsumi, and K. Machida, Pairing symmetry of UPt_3 probed by thermal transport tensors, J. Phys. Soc. Jpn. **83**, 061013 (2014).

[59] F. Lambert, A. Akbari., P. Thalmeier, and I. Eremin, Surface state tunneling signatures in the two-component superconductor UPt_3, Phys. Rev. Lett. **118**, 087004 (2017).

[60] K. Yamada, Y. Nagato, S. Higashitani, and K. Nagai, Rough surface effects on d-wave superconductors, J. Phys. Soc. Jpn. **65**, 1540 (1996).

[61] K. Nagai, Y. Nagato, M. Yamamoto, and S. Higashitani, Surface bound states in superfluid ^3He, J. Phys. Soc. Jpn. **77**, 111003 (2008).

[62] S.-I. Suzuki and Y. Asano, Effects of surface roughness on the paramagnetic response of small unconventional superconductors, Phys. Rev. B **91**, 214510 (2015).

[63] S. Higashitani and N. Miyawaki, Phase transition to a time-reversal symmetry-breaking state in d-wave superconducting films with rough surfaces, J. Phys. Soc. Jpn. **84**, 033708 (2015).

[64] G. Eilenberger, Transformation of Gorkov's equation for type II superconductors into transport-like equations, Z. Phys. **214**, 195 (1968).

[65] The quasiclassical approximation allows us to extract the essential spatial profile (i.e., coherence-length order) from the Green's function by ignoring the rapid oscillation with the Fermi-wavelength order.

[66] Yu. N. Ovchinnikov, Critical current of thin films for diffuse reflection from the walls, Zh. Eksp. Teor. Fiz. **56**, 1590 (1969) [Sov. Phys. JETP **29**, 853 (1969)].

[67] A. A. Golubov and M. Yu. Kupriyanov, Anomalous proximity effect in d-wave superconductors, Pis'ma Zh. Eksp. Teor. Fiz. **67**, 478 (1998) [JETP Lett. **67**, 501 (1998)].

[68] A. A. Golubov and M. Yu. Kupriyanov, Surface electronic scattering in d-wave superconductors, Pis'ma Zh. Eksp. Teor. Fiz. **69**, 242 (1999) [JETP Lett. **69**, 262 (1999)].

[69] N. Schopohl and K. Maki, Quasiparticle spectrum around a vortex line in a d-wave superconductor, Phys. Rev. B **52**, 490 (1995).

[70] M. Eschrig, Distribution functions in nonequilibrium theory of superconductivity and Andreev spectroscopy in unconventional superconductors, Phys. Rev. B **61**, 9061 (2000).

[71] M. Eschrig, Scattering problem in nonequilibrium quasiclassical theory of metals and superconductors: General boundary conditions and applications, Phys. Rev. B **80**, 134511 (2009).

[72] The Y_1^1, Y_2^1, Y_2^2, Y_3^1, Y_3^2, and Y_3^3 pairings correspond to $p_x + ip_y$, $d_{zx} + id_{yz}$, $d_{x^2-y^2} + id_{xy}$, $f_{x(5z^2-1)} + if_{y(5z^2-1)}$, $f_{(x^2-y^2)z} + if_{xyz}$, and $f_{x(x^2-3y^2)} + if_{(3x^2-y^2)y}$-wave pairings, respectively.

[73] The effects of the effective pair potential are determined by the amplitude of s-wave pairs $|\langle f \rangle|$ and the mean free path $\ell = v_F \tau_0$.

[74] The pair potentials for the other chiral SCs are qualitatively the same as those of the Y_2^2 SC because the subdominant s-wave amplitude is not large enough to affect the pair potentials.

[75] At a specular surface of a chiral SC, one of the pair potentials (Δ_1 or Δ_2) becomes zero at the surface. The pair potential proportional to $k_\perp$ becomes zero at the interface, where $k_\perp$ is the perpendicular component of the momentum. In our notation (see Table I), in the Y_l^m SCs with the odd m, the Δ_1 component is proportional to $k_\perp$ (i.e., k_x in our system). On the other hand, in the Y_l^m SCs with the even m, the Δ_2 component is proportional to $k_\perp$.

[76] P. W. Anderson, Theory of dirty superconductors, J. Phys. Chem. Solids **11**, 26 (1959).